Experimental characterization and modelling of adhesive bonded joints under static and non-monotonic fracture loading in the mode II regime

Marco Lamberti, Aurelien Maurel-Pantel, Frederic Lebon

International Journal of Adhesion & Adhesives 124 (2023) 103394

Contents lists available at ScienceDirect

International Journal of Adhesion and Adhesives

journal homepage: www.elsevier.com/locate/ijadhadh

Experimental characterization and modelling of adhesive bonded joints under static and non-monotonic fracture loading in the mode II regime

Marco Lamberti [a,b,*], Aurelien Maurel-Pantel [a], Frederic Lebon [a]

[a] Aix-Marseille University, CNRS, Centrale Marseille, LMA, Marseille, France
[b] ENEA, Brasimone Research Center, Italy

ARTICLE INFO

Keywords:
Double lap shear joint
Metals
Imperfect interface model
Damage evolution

ABSTRACT

Understanding and predicting the behaviour of bonded joints under different loading conditions is certainly an aspect of primary importance. Although numerous experimental studies have been carried out over the last few decades, the shear behaviour of bonded joints under cyclic loading has not been investigated in detail. To fill this gap, an extensive experimental and numerical program of double lap shear bonded joints has been carried out. The double lap shear joints were tested under static and cyclic loading to evaluate and compare the influence of external forces on the adhesive performance. The results are discussed in terms of the force-displacement relationship, shear stress, stiffness, residual displacement, and initial damage. Finally, a method is presented for predicting the actual behaviour of double lap shear bonded joints under different loading conditions using an imperfect interface model with damage evolution. The numerical results are in good agreement with the experimental results for all loading conditions. This work has provided and validated an interesting design tool for adhesive structures.

1. Introduction

In recent decades, the use of adhesives for structural joints in mechanical and civil engineering has increased, e.g. for co-bonding or secondary bonding [1]. The most important properties of adhesive bonds are undoubtedly the absence of holes, which prevents high stress concentration on the bonded surface, the ease and ability to bond different materials such as steel, aluminium and fibre reinforced composites, the speed of installation or replacement of damaged structural elements, the ease of maintenance and the improvement of corrosion protection [2]. These properties, which are essential in the marine industry, mean that this type of joint is considered particularly suitable for the construction of secondary components in aggressive environments, such as wind turbines in offshore structures [3,4]. In addition, many steel structures-built decades ago around the world, such as high-rise buildings, steel monopoles or steel bridges, need to be rehabilitated and repaired [5].

It is well known that the failure mechanisms of bonded joints can be influenced by a number of factors, such as loading conditions, mechanical properties of the adhesive and adherend, adhesive thickness and, undoubtedly, the quality of the bond.

Over the years, severe loading conditions can occur on structural joints consisting of adhesive bonds, causing irreversible deformations that lead to a reduction in the service life of the structure. The presence of major causes of degradation, such as vibration, is an aspect that needs to be investigated. Therefore, a deep and complete understanding of the behaviour of adhesive bonds is essential and fundamental to fully exploit their capabilities in various technical fields such as civil and mechanical engineering.

Since the beginning of the twentieth century, several scientists have carried out experimental and numerical research on bonded joints. In 1938, Volkersen [6] developed a simple model to study the shear stress at the interface of single-lap bonds, assuming a pure tension hypothesis and neglecting bending due to the presence of eccentricity. A few years later, Goland and Reissner [7], in their analytical work, introduced the bending behaviour of the adherend, before neglecting it, and proposed a model based on the stress analysis of the beam. Subsequently, Hart-Smith L.J [8]. simplified the complicated stress-strain behaviour using a bilinear or elastoplastic curve, which was an important breakthrough and made the model an effective tool for aircraft joint design.

In recent years, Banea and da Silva [9,10] have provided a comprehensive review of the experimental and numerical behaviour of

* Corresponding author. Aix-Marseille University, CNRS, Centrale Marseille, LMA, Marseille, France.
E-mail addresses: lamberti@lma.cnrs-mrs.fr, marco.lamberti@enea.it (M. Lamberti), maurel@lma.cnrs-mrs.fr (A. Maurel-Pantel), lebon@lma.cnrs-mrs.fr (F. Lebon).

https://doi.org/10.1016/j.ijadhadh.2023.103394
Received 21 September 2022; Received in revised form 3 April 2023; Accepted 2 May 2023
Available online 9 May 2023

bonded joints in composite materials and have also described the main causes affecting the performance of bonded joints: surface treatment, joint configuration, geometrical and material parameters, and failure mode.

Many experimental studies have also been carried out: da Silva et al. [11] investigated the effect of adhesive type and thickness on the lap shear strength of the single-lap joint and concluded that the lap shear strength increases as the bond line becomes thinner and the adhesive becomes tougher. Seong et al. [12] experimentally investigated the effects of various parameters such as bonding pressure, overlap length, adhesive thickness and material type on the failure load and mode of carbon composite-aluminium bonded single-lap joints. Reis et al. [13] compared the tensile shear strength of different adhesives using single lap joints. They found that the shear strength of the joints was influenced by the stiffness of the bond and the shear strength of the adhesive. Vallée et al. [14] investigated the influence of stress reduction methods on the strength of bonded double lap shear joints made from brittle adhesives. Their experimental tests showed that the increase in strength from these stress-reduction methods was negligible. Li et al. [15] experimentally investigated the tensile performance and the influence of various lap parameters on the bond strength and failure mode of bonded CFRP joints. The experimental tests showed that the lap shear strength for the brittle adhesive studied was not directly proportional to the overlap length, adhesive thickness, width of the bonded area and the scarf angle.

Other researchers have focused their studies on the fatigue behaviour of bonded joints. Kim et al. [16] experimentally investigated the static and fatigue behaviour of lap joints for composite structures and evaluated the bond strength and residual strength. Then, Jen et al. [17,18] analysed the effects of overlap length and adhesive thickness on the fatigue strength of lap joints using experimental tests. It was found that the fatigue strength decreased as the overlap length increased. In addition, the fatigue performance of adhesive single-lap joints made of thick composite materials [19] or carbon nanostructured joints [20] has also been investigated. The experimental and numerical studies by Ayatollah [21,22] on the fatigue behaviour of adhesive bonded flat and non-flat lap joints showed that non-flat lap joints tolerate higher static loads and exhibit higher fatigue life due to dominant fatigue crack propagation. Subsequently, Pereria [23] carried out experimental fatigue tests on single lap joints made by bonding steel plates with Araldite 420. The results emphasised that the fatigue life is slightly dependent on the strain rate.

Other experimental studies have shown that adhesive thickness [24] and the addition of nanoparticles to the adhesive [25] significantly affect the fatigue performance [26] of bonded joints. The effect of adhesive thickness on fatigue crack growth has also been investigated experimentally and numerically by Pascoe [27]. He concluded that the energy required per unit of crack growth does not depend on the adhesive thickness, but only on the energy available for crack growth. Low cycle fatigue tests [28] have been carried out on the adhesive bonded hollow cylindrical butt joints in stress controlled mode and the effects of stress amplitude and loading frequency on the fatigue life of the specimens have been analysed.

In the field of numerical models capable of accounting for the presence of some imperfections in the adhesive layers, the use of model updating in the adhesive region has also been investigated [29–31]. Jahani and Nobari [29] determined the mechanical properties of the adhesive (Young's modulus and shear modulus) using the modal-based direct model updating method and experimental modal data. The results showed that the thickness and length of the adhesive joint affect these properties. The effect of defects on the equivalent identified Young's modulus and shear modulus of structural bonded joints was investigated by Meshki et al. [30]. A year later, Pazand and Nobari [31] investigated the effect of damage in both linear and nonlinear regions of the adhesive behaviour using the inverse eigen sensitivity identification procedure. The results indicated that debonding damage has a decreasing effect on adhesive damping in both linear and nonlinear regions, and that the reduction becomes more pronounced as the percentage of damage increases. Although the study of bonded joints from both numerical and experimental points of view is widespread, there is a lack of methodology capable of combining these two aspects and providing a useful tool for analysing the behaviour of bonded joints subjected to non-monotonic loading conditions and capable of simulating different types of damage evolution.

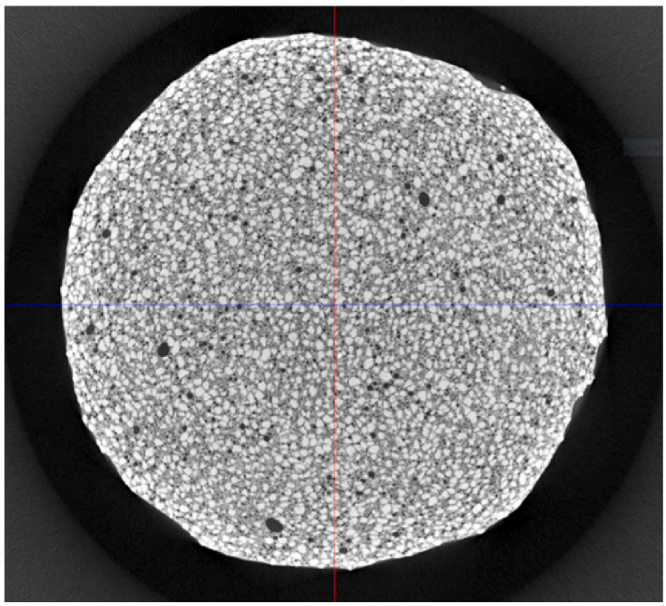

Fig. 1. CT scan image of a SikaDur adhesive joint. The scanning step used an X-ray source with a voxel size of 30 μm, a voltage of 150 kV and a current of 18 μA. The image resolution is 1920 × 1536 pixels. The instrument used is an EasyTom XL Ultra 150/160 (μCT) from RX Solution.

In this context, in a first paper [4], the authors successfully demonstrated the possibility of describing the evolution of the mechanical properties of bonded joints under monotonic and non-monotonic loading in Mode I, using an imperfect interface model with evolving damage. This model was identified using elementary tensile tests and validated on a complex bonded GRP beam structure.

In the present work, the difference between Mode I and Mode II damage evolution was assumed and the need to increase the knowledge of Mode II was presented as a point of perspective.

The authors propose to identify their own imperfect interface model with Mode II damage evolution for monotonic and non-monotonic loading. To achieve this goal, an extensive experimental charactier on bonded double lap shear joints has been carried out. The effects of different loading conditions on the performance of bonded joints have been studied. Different loading regimes have been applied: monotonic and cyclic to obtain different types of damage evolution. The experimental results show that the presence of cyclic loading affects the progressive evolution of damage in adhesive joints. In order to reproduce the experimental results, the predictive imperfect interface model has been considered. This model has been derived by an asymptotic approach applied to a composite structure consisting of two elastic solids bonded by a third thin one, characterised by a non-linear behaviour. The adhesive layer is considered to be microcracked by adopting Kachanov-type assumptions [32–35]. This imperfect interface model can take into account several adhesive parameters such as thickness, porosity, presence of initial damage and its evolution. The experimental tests allowed to identify the main mechanical parameters of the theoretical formulations, including the adhesive stiffness and the initial damage. Finally, the model was implemented in a finite element software and its performance was demonstrated by reproducing the experimental results with good agreement.

Table 1
Mechanical properties of epoxy adhesive (SikaDur-30 [36]).

	Test Standards	Value
Young's Modulus in compression, E_C	ASTM D 695	9.6 GPa
Young's Modulus in tension, E_T	ISO 527	11.2 GPa
Compressive Strength, σ_C	EN 196	70–80 MPa (at 15 °C) and 85–95 MPa (at 35 °C)
Tensile Strength, σ_N	DIN EN ISO 527-3	24–27 MPa (at 15 °C) and 26–31 MPa (at 35 °C)
Shear Strength, τ	FIP 5.15	14–17 MPa (at 15 °C) and 16–19 MPa (at 35 °C)

Table 2
Mechanical properties of steel.

	Value
Tensile Yield Strength, σ_S	235 MPa
Young's Modulus, E_S	210 GPa
Poisson's ratio, ν_S	0.3

2. Experimental program

2.1. Adhesive and substrate

The epoxy resin-based adhesive used in this study was Sikadur-30 manufactured by Sika [36]. This adhesive is a thixotropic two-component structural adhesive consisting of an epoxy resin and special fillers, as shown in Fig. 1, and is designed for bonding at temperatures between 8 °C and 35 °C.

Curing takes place within 7 days at room temperature. After this time, the bulk adhesive achieves the following mechanical properties as specified by the manufacturer [36] and listed in Table 1.

Bonded joints were made using S235 steel plates with different geometric dimensions, the mechanical properties of which are given in Table 2.

2.2. Experimental set-up

An extensive experimental program on double lap shear adhesive joints has been carried out at the Laboratory of Mechanics and Acoustics (LMA) in Marseille, France. A total of 38 double lap shear bonded joints were designed and tested under static and cyclic loading.

The geometric configuration of the lap specimens was selected based on ASTM D3528-96 [37]. The dimensions of the specimens conform to Type B of the standards as shown in Fig. 2.

The specimens consist of four steel plates, two of 112 × 26 × 4 mm and two of 50 × 26 × 2 mm respectively, bonded together by adhesive layers with an overlap of 20 mm. Two sets of specimens were prepared with different adhesive thicknesses: 2 and 4 mm.

It is important to underline that the choice of these thicknesses is based on the feasibility on site by specialised workers, especially for the connection of secondary structures in offshore wind turbines. In fact, thin and uniform adhesive thicknesses are easy to obtain in specialised laboratories, otherwise it becomes difficult to produce them on site.

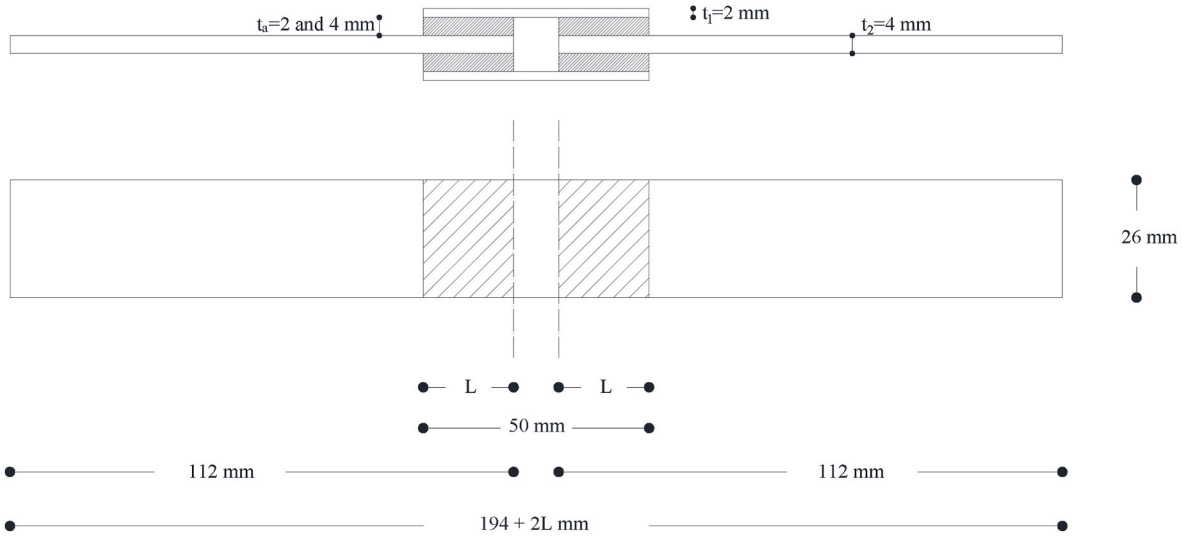

Fig. 2. Shape and dimensions of the Type B sample (ASTM D 3528–96).

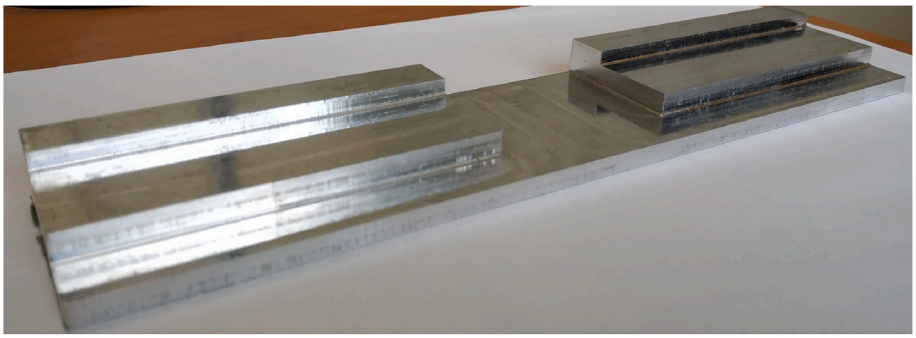

Fig. 3. Ad hoc device made of aluminium for making double lap shear bonded joints.

Fig. 4. Double lap shear adhesive specimens.

An aluminium fixture, shown in Fig. 3, was designed and built to control and apply the glue thickness and to guarantee coplanarity between the steel sheets.

The following procedure was used to prepare the samples. First, the small steel plate of 50 mm in length is positioned in the centre of the aluminium fixture. Then the adhesive is applied to it and the two 112 mm long steel plates are added and placed in the appropriate positions. Once the adhesive has cured, the first half of the sample can be removed. Another plate is then placed in the corresponding area of the fixture and the bonding process is repeated with the previous half-part inverted.

The samples shown in Fig. 4 were polymerised at room temperature for 7 day before testing. To ensure perfect adhesion, the steel surfaces were thoroughly cleaned with acetone.

As shown in Fig. 5(a–d), the experimental tests were carried out using an MTS 322 test frame servo-hydraulic testing machine with a load capacity of 100 kN. The specimens, fixed at their ends, were tested up to failure at a rate of 0.5 mm/min using a suitable multi-step displacement control.

A 2D DIC system (Aramis) was installed to evaluate the displacement and strain fields of the adhesive interfaces. During the experimental tests, the corresponding displacement and strain measurements of the adhesive thicknesses are continuously acquired by processing in-situ images taken by a 2D DIC system from one side. A camera monitored the adhesive layers of the specimen during the loading process.

The strain fields are measured using an optical extensometer technique. Images of the speckle pattern are taken at regular intervals during the test using a PCO. edgesCMOS camera with a 5.5 megapixel sensor. The frame rate was set to 3 frames per second (fps) for the uniaxial tensile test.

The acquired speckle pattern images were then analysed using the GOM ARAMIS 6.5 Direct Image Correlation (DIC) software by selecting two points on the coupon surface and using the differential displacement between them to estimate the deformation of the sample. When processing these images, the subset size was set to 15 × 15 pixels.

2.3. Static and non-monotonic tests

Specifically, the double lap shear joint test program included three loading regimes: monotonic and two types of cyclic loading. A total of 27

Fig. 5. Double lap shear tests for different adhesive thicknesses: a-b) 4 mm and c-d) 2 mm.

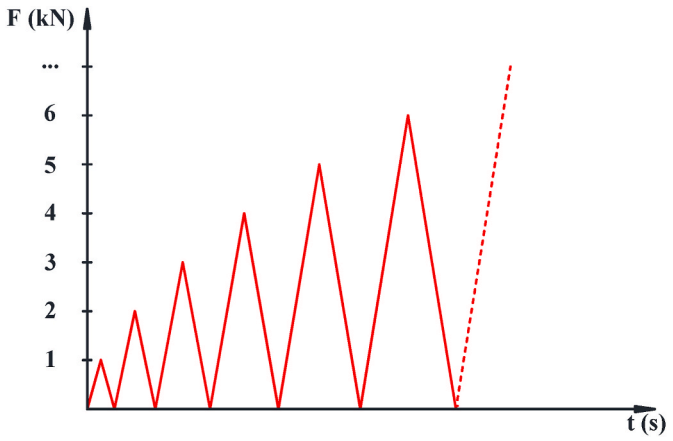

Fig. 6. Force versus time curve for double lap shear joints under the first path of cyclic loading condition.

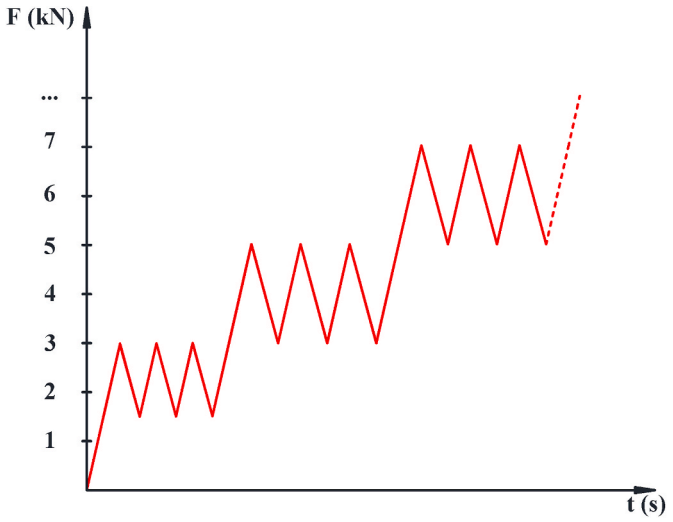

Fig. 7. Force versus time curve for double lap shear joints under the second path of cyclic loading condition.

specimens were subjected to monotonically increasing quasi-static loading to failure for two adhesive thicknesses of 2 and 4 mm, performed under displacement control. Once the failure load values for each specimen type had been determined from the monotonic tests, a total of 11 cyclic tests were performed. Two different load paths were adopted in the experimental program. The first load path is characterised by a 1 kN increase in the maximum value of the force reached in each cycle until failure, as shown in Fig. 6. In the second loading path, summarised in Fig. 7, three series of three cycles of loading and unloading were carried out, starting from 15% of the average failure load to 30%, from 30% to 50% and from 50% to 70%. After 70%, the load changes monotonically until failure.

The two path loads chosen were chosen to evaluate the influence of the loading conditions on the bond behaviour. In fact, during the life of the structure, the bonded joints could be subjected to different loading conditions. For example, a seismic event may occur that is characterised by actions of different magnitudes (a small number of cycles of different intensities [38]). The chosen path loads allow to assess the variation of damage at different levels of loading.

3. Experimental results

This section presents and discusses the experimental results of the double lap shear joints under different loading conditions. Numerous tests under monotonic conditions were carried out to evaluate the mechanical properties of the bonded joints for the two thicknesses.

Table 3
Static response of double lap joints with an adhesive thickness of 4 mm.

ID#	F_u [kN]	τ_{av} [MPa]	δ_u [mm]	K [kN/mm]	τ_u [MPa]	G [GPa]
M4#1	9.98	9.59	0.140	72.08	–	–
M4#2	13.53	13.01	0.192	71.52	–	–
M4#3	11.48	11.04	0.162	68.09	–	–
M4#4	10.09	9.71	0.134	75.87	22.02	6.36
M4#5	12.48	12.00	0.177	70.86	19.08	7.32
M4#6	9.29	8.94	0.129	72.54	22.03	3.81
M4#7	9.89	9.51	0.144	69.76	–	–
M4#8	8.61	8.28	0.118	74.42	10.66	5.30
M4#9	11.81	11.35	0.158	73.41	16.40	3.90
M4#10	8.64	8.31	0.119	74.66	10.54	2.67
M4#11	8.99	8.64	0.115	76.99	10.01	3.96
M4#12	9.09	8.74	0.122	76.13	10.94	5.15
M4#13	10.24	9.84	0.149	69.30	12.28	4.73
Average	***10.32***	***9.92***	***0.143***	***72.74***	***14.88***	***4.80***
dev.st	***1.49***	***1.43***	***0.023***	***2.69***	***4.77***	***1.34***

Table 4
Static response of double lap joints with an adhesive thickness of 2 mm.

ID#	F_u [kN]	τ_{av} [MPa]	δ_u [mm]	K [kN/mm]	τ_{max} [MPa]	G [GPa]
M2#1	9.90	9.52	0.119	84.30	19.00	6.35
M2#2	11.22	10.79	0.138	81.85	17.68	6.16
M2#3	9.29	8.93	0.116	81.72	–	–
M2#4	13.41	12.90	0.170	79.70	25.86	4.44
M2#5	10.50	10.09	0.135	79.28	17.11	5.48
M2#6	14.44	13.89	0.197	73.59	–	–
M2#7	14.22	13.67	0.193	73.81	23.67	3.66
M2#8	10.89	10.47	0.144	77.44	–	–
M2#9	11.58	11.14	0.155	76.07	–	–
M2#10	9.22	8.74	0.122	78.18	19.41	6.13
M2#11	10.81	10.40	0.138	78.59	18.06	5.40
M2#12	15.24	14.66	0.208	74.42	19.87	4.93
M2#13	10.85	10.43	0.151	72.95	–	–
M2#14	11.26	10.83	0.153	73.96	17.17	5.43
Average	***11.63***	***11.18***	***0.153***	***77.56***	***19.76***	***5.35***
dev.st	***1.86***	***1.80***	***0.028***	***3.45***	***2.87***	***0.85***

The experimental results for the static tensile tests are summarised in Tables 3 and 4. In the following tables, each test is identified by the label "*Xy#m*", where *X* indicates the type of action applied (M = monotonic, CF = first cyclic load path, CS = second cyclic load path), *y* is the adhesive thickness in mm and *m* is the progressive test number.

The other symbols have the following meaning: F_u indicates the ultimate experimental force achieved, τ_{av} the average shear stress along each adhesive layer, calculated by dividing the ultimate force by two times the bond area, δ_u the displacement corresponding to the ultimate load, *K* the stiffness of the joint evaluated from the slope the of the experimental curve, τ_u the ultimate shear stress achieved along the adhesive layer and *G* the adhesive shear modulus.

More specifically, the stiffness *K* was evaluated by linear interpolation of the experimental force-displacement curve. The ultimate adhesive shear stress τ_u and the shear modulus *G* were quantified from the displacement field recorded by the measurement system.

In fact, the use of displacement field data allows a more precise evaluation of the aforementioned quantities, as they are less affected by the choice of the mesh size of the adhesive layer in the extrapolation data process. From the displacement field, is possible to evaluate the shear deformation, γ, by dividing the difference in the displacement of two points, Δu, for the respective distance, *h*, as shown in Eq. (1). It is well known that the shear stress τ is obtained by multiplying the shear deformation by the adhesive shear modulus *G* which is an unknown at the beginning. According to the formula in Eq. (2), the average value of

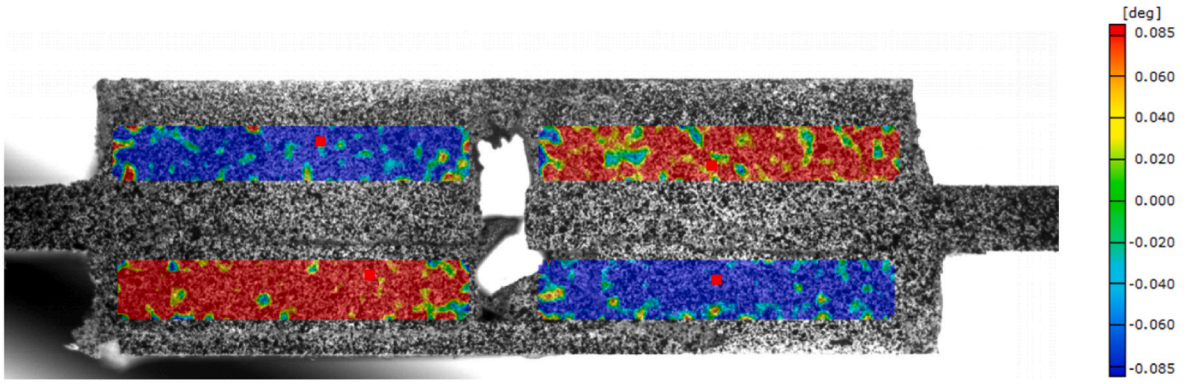

Fig. 8. Shear deformation field for M4#12 double joint test with 4 mm adhesive thickness.

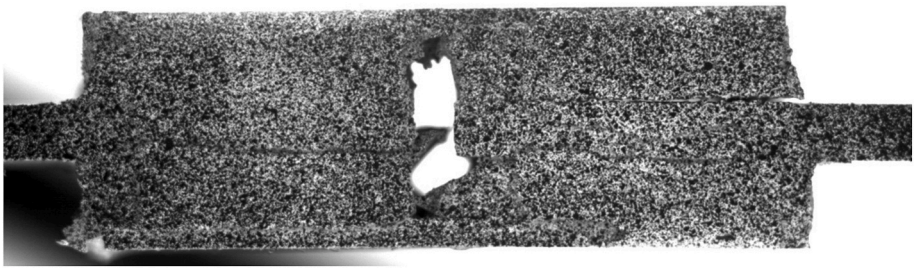

Fig. 9. Detailed view of the failed adhesive region of the test M4#12.

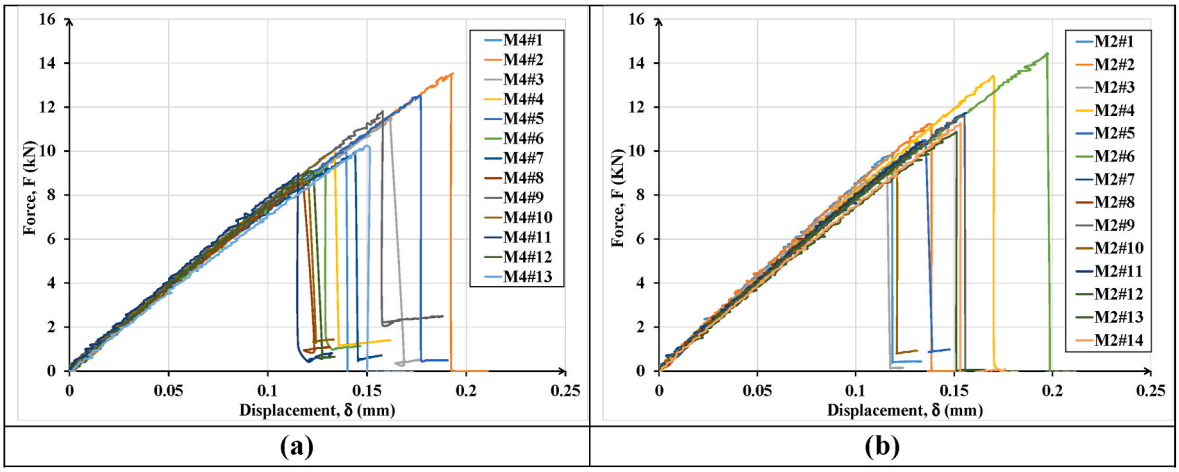

Fig. 10. Force-displacement curve for double lap shear bonded joints: a) M4; b) M2.

the shear stress τ_m along the adhesive layer can be calculated by setting the value of G, where n is the total number of elements into which the adhesive layer is divided (with $i = 1,2 \ldots,n$).

The exact value of G is obtained when the mean value of shear stress τ_m, evaluated from the displacement field (Eqs. (1) and (2)), is equal to the mean shear stress, τ_{av}, evaluated by dividing the total external force, F, by the total adhesive surface S (Eq. (3)).

$$\gamma = \frac{u_1 - u_2}{h} = \frac{\Delta u}{h} \tag{1}$$

$$\tau_m = \frac{1}{n}\sum_{i=1}^{n}\tau_i = \frac{G}{n}\sum_{i=1}^{n}\gamma_i \tag{2}$$

$$G \rightarrow \tau_m = \frac{F}{2A} \tag{3}$$

Fig. 8 shows an example of the shear strain field obtained by direct image correlation for the double lap shear bond labelled M4#12 at a high force level of 8.01 kN. As can be seen in Fig. 8, each adhesive layer is characterised by positive values of shear strain γ represented in red or negative values in blue, thus highlighting the absence of bending during the application of the external load.

Indeed, some small presence of positive shear strains in the blue region and vice versa can be seen in Fig. 8, due to the presence of small imperfections in the adhesive surface that make the surface not perfectly smooth.

The detailed view of the failed region of test M4#12 is shown in Fig. 9.

Finally, force vs displacement curves for tests M4 and M2 are shown in Fig. 10.

The results of the monotonic tests showed a substantially equal slope of the load-displacement curves to failure. For specimen M4#4, the

Table 5
Mechanical response of specimen CF4 in terms of residual displacement, stiffness and percentage of ultimate displacement for each cycle (adhesive thickness equal to 4 mm).

Test	cycle	1	2	3	4	5	6	7	8	9	10
	details										
CF4#1	**F (kN)**	1.02	2.01	3.00	3.99	5.06	6.01	6.99	8.06	9.01	9.35
	***w* (μm)**	1.25	1.54	1.77	3.31	3.62	4.33	3.27	8.05	8.44	–
	K_a (kN/mm)	84.40	76.72	77.08	77.68	77.99	77.68	77.89	78.19	77.78	77.44
	K_b (kN/mm)	85.94	78.98	78.29	79.14	78.47	78.61	78.62	78.30	77.83	–
	%w	0.99	1.23	1.41	2.63	2.87	3.44	2.60	6.39	6.70	–
CF4#2	**F (kN)**	0.97	1.99	3.02	4.01	5.05	5.99	7.02	8.00	7.29	
	***w* (μm)**	2.46	3.26	1.48	3.22	3.15	1.28	3.49	4.16	–	–
	K_a (kN/mm)	79.67	85.52	81.05	81.67	81.30	80.95	80.31	79.86	79.32	–
	K_b (kN/mm)	66.44	84.65	83.29	82.29	81.25	80.75	80.78	80.06	79.59	–
	%w	2.55	3.16	1.43	3.12	3.06	1.25	3.38	4.03	–	–
CF4#3	**F (kN)**	1.10	1.90	3.06	4.11	5.05	5.95	7.02	8.02	8.90	9.88
	***w* (μm)**	0.18	1.96	0.53	0.55	0.32	2.38	3.89	2.11	7.67	–
	K_a (kN/mm)	74.06	81.84	84.2	82.99	82.82	82.59	80.98	80.85	80.60	79.78
	K_b (kN/mm)	79.56	82.37	83.62	83.34	83.12	82.65	81.38	80.78	80.38	–
	%w	0.14	1.54	0.42	0.43	0.25	1.87	3.06	1.65	6.03	–

Table 6
Mechanical response of specimen CF2 in terms of residual displacement, stiffness and percentage of ultimate displacement for each cycle (adhesive thickness equal to 2 mm).

Test	cycle	1	2	3	4	5	6	7	8	9	10	11	12	13
	details													
CF2#1	**F (kN)**	1.13	1.99	2.97	3.92	4.94	5.90	7.07	7.96	8.99	9.97	10.94	9.82	–
	***w* (μm)**	2.61	1.39	3.24	3.80	4.40	4.48	6.78	8.26	8.35	9.49	10.06	–	–
	K_a (kN/mm)	70.86	75.41	78.87	77.65	76.89	77.46	76.97	77.01	76.97	76.84	76.47	76.31	–
	K_b (kN/mm)	79.88	78.11	76.09	77.19	77.76	77.74	77.62	77.65	77.10	77.01	76.78	–	–
	%w	1.86	0.99	2.31	2.71	3.14	3.19	4.84	5.89	5.95	6.76	7.17	–	–
CF2#2	**F (kN)**	1.03	2.04	2.93	3.94	5.02	6.01	7.03	7.98	9.03	10.01	11.00	12.02	10.61
	***w* (μm)**	0.00	1.21	1.25	2.43	1.55	1.62	2.92	3.79	2.21	4.83	8.69	7.21	–
	K_a (kN/mm)	84.55	87.59	90.34	87.64	87.78	87.12	86.93	87.03	85.47	85.75	85.41	85.5	84.90
	K_b (kN/mm)	85.16	89.06	86.36	90.02	87.84	88.20	87.44	86.93	86.37	85.99	85.77	85.14	–
	%w	0.00	0.93	0.96	1.86	1.18	1.24	2.24	2.90	1.69	3.70	6.64	5.52	–

Table 7
Mechanical response of specimen CS4 in terms of residual displacement, stiffness and percentage of ultimate displacement for each cycle (adhesive thickness equal to 4 mm).

Test	cycle	15–30%			30–50%			50–70%		
	details	1	2	3	1	2	3	1	2	3
CS4#1	**F_1 (kN)**	2.96	3.03	3.01	4.81	5.02	5.00	7.16	7.20	7.04
	F_0 (kN)	1.54	1.48	1.54	2.97	3.01	3.03	4.93	4.99	5.08
	***w* (μm)**	1.49	0.69	0.64	0.47	2.76	1.97	3.61	3.65	1.59
	K_a (kN/mm)	78.67	87.14	79.00	80.08	82.05	82.27	78.23	79.23	78.95
	K_b (kN/mm)	83.84	82.59	82.04	81.59	82.81	81.51	80.75	80.46	77.96
	%w	1.24	0.58	0.53	0.39	2.29	1.63	2.99	3.28	1.32
CS4#2	**F_1 (kN)**	2.90	2.95	3.07	4.92	4.99	5.04	7.00	7.01	7.04
	F_0 (kN)	1.65	1.50	1.43	2.85	3.00	2.92	5.00	5.06	4.92
	***w* (μm)**	3.08	2.76	3.25	3.08	5.27	4.72	6.11	6.97	5.65
	K_a (kN/mm)	80.36	78.11	81.30	81.16	86.16	82.16	79.76	78.48	80.64
	K_b (kN/mm)	83.48	82.84	83.58	81.29	83.97	82.59	82.15	82.52	80.11
	%w	2.17	1.94	2.29	2.38	3.71	3.32	4.31	4.91	3.98

maximum debonding load value of 13.53 kN was recorded, slightly higher than that recorded for the other specimens characterised by a thickness of 4 mm and an average ultimate load value of 10.32 kN. The average ultimate displacement for specimen M4 is 0.143 mm. The M2 specimens, characterised by an adhesive thickness of 2 mm, have a higher average ultimate load of 11.63 kN and a global stiffness of 77.41 kN/mm. The debonding displacement reaches a mean value of about 0.153 mm. For the adhesive shear modulus, a mean value of 5076 MPa was obtained for all samples. In addition, the average maximum shear stress of the adhesive layer obtained is equal to 14.88 MPa for specimens with an adhesive thickness of 4 mm, while it is equal to 19.76 MPa for specimens with an adhesive thickness of 2 mm, confirming once again the greater resistance capacity of the specimens with a smaller adhesive thickness.

On the other hand, the main experimental results relating to cyclic tests are given in Tables 5–8. In these tables, the values of the experimental tests are summarised in terms of axial force, denoted by *F*, where the subscripts *0* and *1* represent the initial and final points of the load/unload curve; *w* represents the irreversible elongation of the adhesive and *%w* is the percentage of the residual displacement evaluated with

Table 8
Mechanical response of specimen CS2 in terms of residual displacement, stiffness and percentage of ultimate displacement for each cycle (adhesive thickness equal to 2 mm).

Test	cycle	15–30%			30–50%			50–70%		
	details	1	2	3	1	2	3	1	2	3
CS2#1	F_1 (kN)	3.03	3.06	2.94	5.05	5.00	4.99	7.02	6.95	6.99
	F_0 (kN)	1.49	1.49	1.54	2.99	2.98	2.98	5.00	4.88	4.97
	w (μm)	2.27	1.85	3.03	3.99	1.65	3.47	5.18	6.02	7.46
	K_a (kN/mm)	82.73	83.67	79.18	83.38	82.89	83.77	83.32	82.89	89.76
	K_b (kN/mm)	86.39	84.32	87.86	86.29	81.38	85.17	85.48	86.29	87.94
	%w	1.01	0.82	1.35	1.78	0.73	1.54	2.30	2.68	3.31
CS2#2	F_1 (kN)	3.03	2.84	3.10	5.04	5.02	5.10	6.87	6.99	6.91
	F_0 (kN)	1.54	1.40	1.43	2.99	2.98	5.03	5.06	4.96	5.08
	w (μm)	0.00	0.62	0.41	2.57	2.41	2.12	2.89	1.96	4.46
	K_a (kN/mm)	83.78	76.91	86.32	83.15	87.64	86.50	81.27	81.19	80.53
	K_b (kN/mm)	79.40	84.97	83.48	85.91	84.86	84.04	83.34	81.68	83.80
	%w	0.00	0.60	0.39	2.48	2.33	2.05	2.79	1.89	4.30
CS2#3	F_1 (kN)	3.14	3.00	2.97	4.93	5.08	4.90	7.00	7.06	7.00
	F_0 (kN)	1.54	1.39	1.55	3.02	2.95	2.99	4.96	5.01	4.96
	w (μm)	0.14	0.00	0.83	0.00	2.80	2.17	2.86	5.09	4.06
	K_a (kN/mm)	81.65	81.45	80.68	82.27	84.96	86.54	82.73	82.87	88.27
	K_b (kN/mm)	84.38	82.09	85.95	81.76	86.46	85.08	83.91	86.21	84.66
	%w	0.12	0.00	0.73	0.00	2.45	1.89	2.50	4.44	3.55
CS2#4	F_1 (kN)	3.08	3.00	3.04	4.97	5.03	5.05	7.09	6.98	5.04
	F_0 (kN)	1.54	1.56	1.43	3.06	2.88	2.94	5.02	4.99	5.04
	w (μm)	1.09	0.92	2.09	3.83	5.52	4.46	5.85	4.06	7.99
	K_a (kN/mm)	82.11	82.35	80.37	83.41	84.92	84.01	82.96	81.19	84.59
	K_b (kN/mm)	85.02	84.57	86.94	87.18	89.46	87.54	86.29	83.57	87.42
	%w	0.63	0.53	1.22	2.23	3.21	2.70	3.38	2.36	4.64

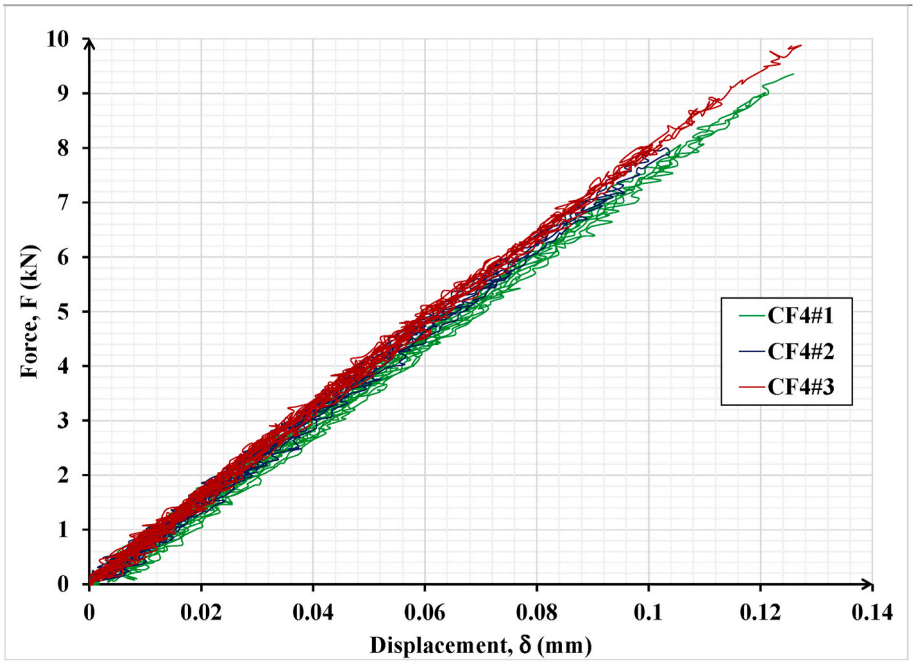

Fig. 11. Force-displacement curve for double lap shear adhesive joints CF4.

respect to the displacement corresponding to the debonding load.

The value of the stiffness *K* has been evaluated for both the ascending branch K_a and the descending branch K_b thanks to the linear interpolation of load/unload curves.

The experimental load-displacement curve results for the cyclic tests (first path load) CF4 and CF2 are shown in Figs. 11–12, respectively.

The experimental observations show a slight decrease in stiffness after the first cycles due to an increase in damage to the adhesive components.

For the cyclic tests CF4 and CF2, the residual displacement increases with each cycle, resulting in a significant value with respect to the final displacement already from the 4–5° cycle. The maximum residual displacement, *w,* reached for specimens CF4 is equal to 0.0106 mm while for the CF2 it is equal to 0.0869 mm. In both cases, the tests ended with similar failure loads of monotonic cases.

The experimental load-displacement relationships related to tests CS4 and CS2 under the second path load of cyclic actions are shown in Figs. 13–14, respectively.

The experimental evidence for tests CS2 and CS4 shows that the residual displacement *w* is negligible for the cycles between 15% and

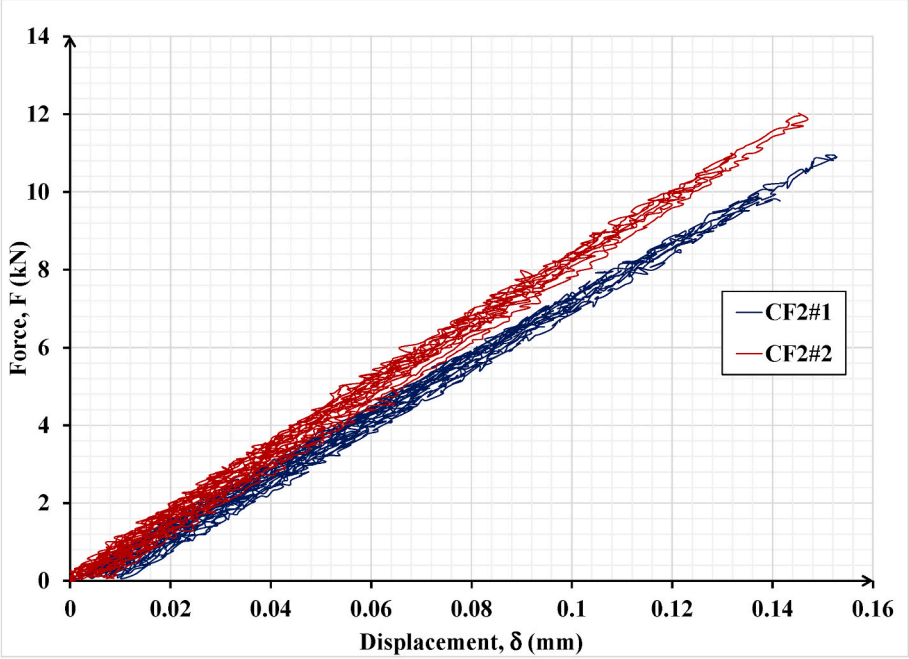

Fig. 12. Force-displacement curve for double lap shear adhesive joints CF2.

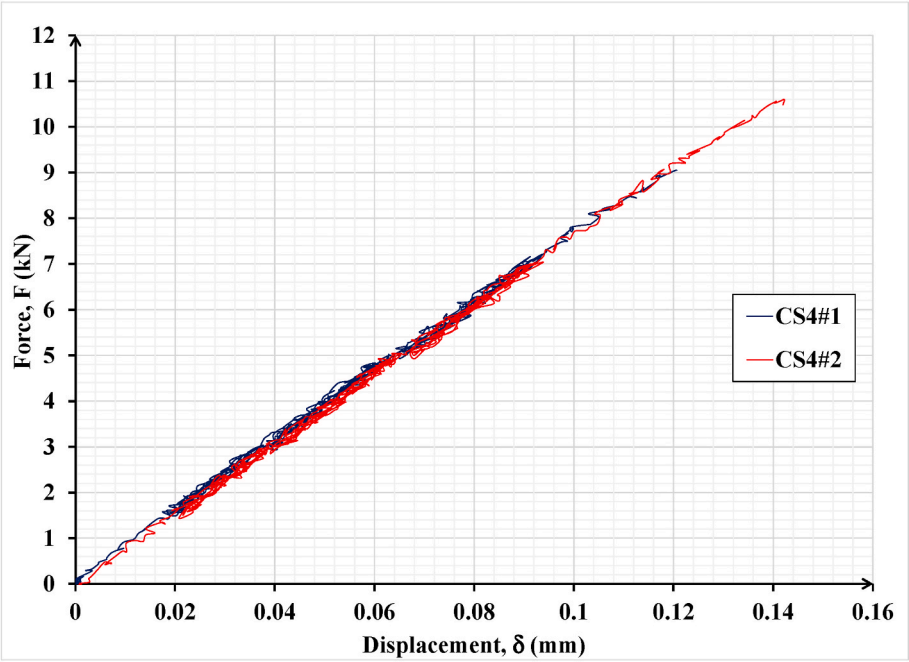

Fig. 13. Force-displacement curve for double lap shear adhesive joints CS4.

30% of the average ultimate load equal to 10 kN. It is important to note that the residual displacements are calculated as the difference between the displacements before and after the loading and unloading paths and represent the damage to the adhesive interface.

The residual displacement becomes large when cycles with higher load levels (range 50–70% of the reference load) have been applied, ranging between 0.00296 mm and 0.00697 mm, and the corresponding percentage of final displacement reaches a value between 3 and 5%.

After the final loading and unloading cycles, the tests were terminated with a monotonic load path. During this step, the bond behaviour was very similar to that observed during the monotonic tests, undoubtedly due to the low series and number of load cycles applied.

Finally, the results show that the mechanical properties of the double lap shear bond are influenced by the adhesive thickness in terms of strength and stiffness. Failure occurs after the initiation of a crack and its instantaneous propagation, which involves the separation of the bonded metallic elements.

Figs. 15–16 show the images taken by the camera at failure for the cyclic specimens for both thicknesses; 4 and 2 mm.

Figs. 17–18 show the images taken by the camera at failure for the second path cyclic loading specimens for both thicknesses, 4 and 2 mm.

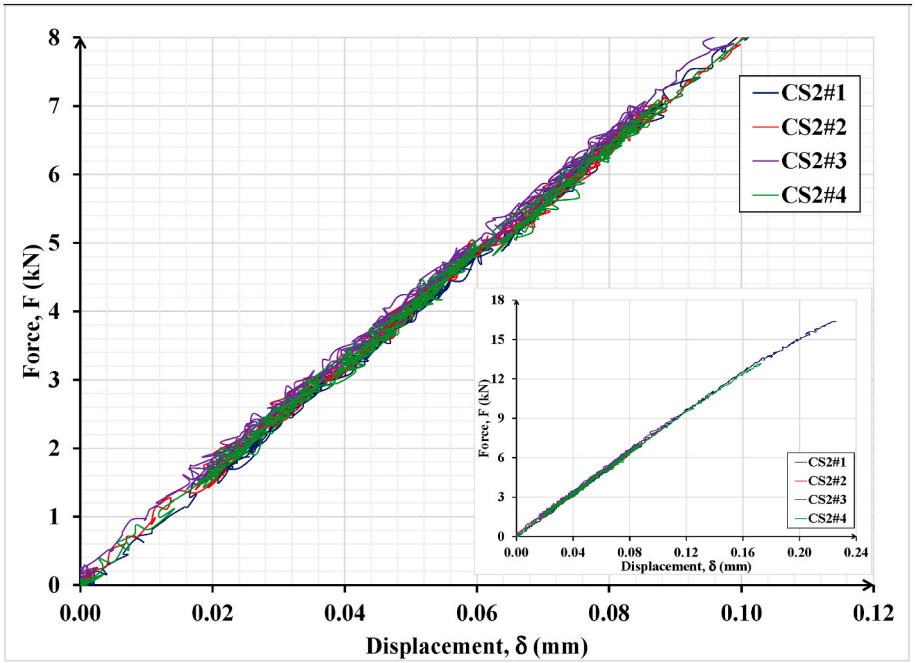

Fig. 14. Force-displacement curve for double lap shear adhesive joints CS2.

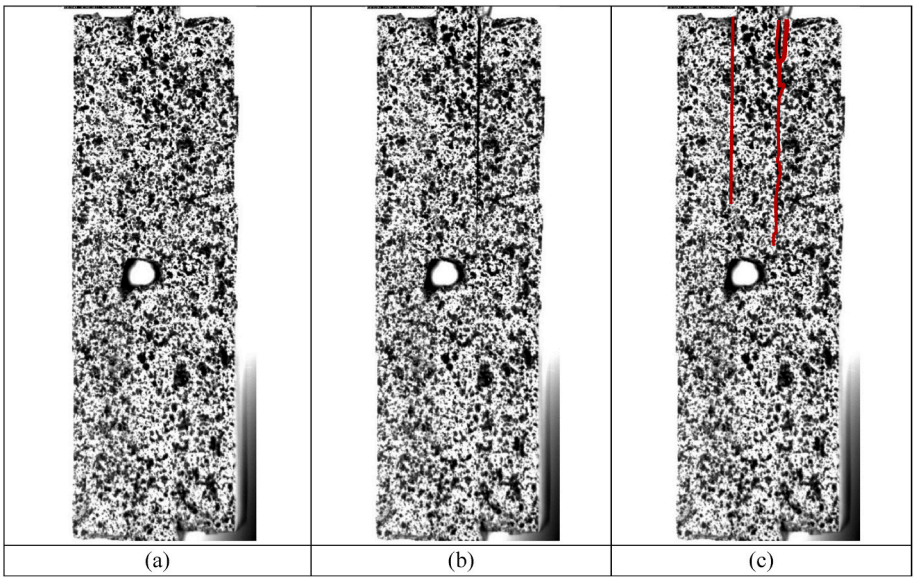

Fig. 15. Detailed view of the failed adhesive area, test CF4#3: a) absence of cracks before failure; b-c) presence of cracks at failure.

4. Numerical modelling using an imperfect interface model

An imperfect interface model proposed by the authors is presented in this section. The model has been formulated by combining the homogenisation technique and the asymptotic approach within the framework of small perturbations [39–43]. Unilateral contact conditions and damage evolution of the adhesive interface characterise the proposed predictive model. According to the approach introduced in Refs. [44, 45], the thin adhesive interphase located between the two adherents is considered as a microcracked material that is subject to a degradation process that evolves during the loading process. The degradation process is guaranteed by the presence of a real microstructure of the adhesive that takes into account several families of microcracks with randomly distributed lengths and orientations. According to the homogenisation technique of the Kachanov type [32–35], based on the Eshelby problem, an idealised microcracked adhesive layer can be obtained. This leads to considering the adhesive interphase of thickness, named ε, between the two adherents as a homogenised material.

Within this non-interactive approximation framework [33], an equivalent length of the microcrack family, called l, represents the family of microcracks with parallel orientation to the bond plate and is retained as representative of the macroscale behaviour of the adhesive. For this reason, the effective mechanical properties are a function of the microcrack density, ρ, which is strictly related to the crack length, l, and the volume, V, as reported in Eq. (4) [42].

$$\rho = \frac{l^3}{V} \tag{4}$$

The crack density, ρ, can evolve over time and thus represents a real damage parameter. For this reason, an evolution law can be formulated

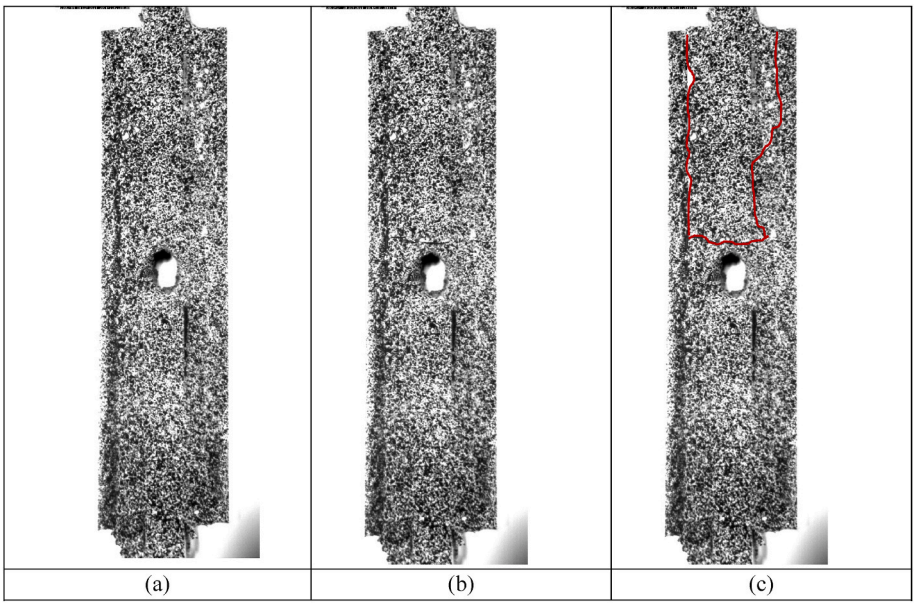

Fig. 16. Detailed view of the failed adhesive area, test CF2#1: a) absence of cracks before failure; b-c) presence of cracks at failure.

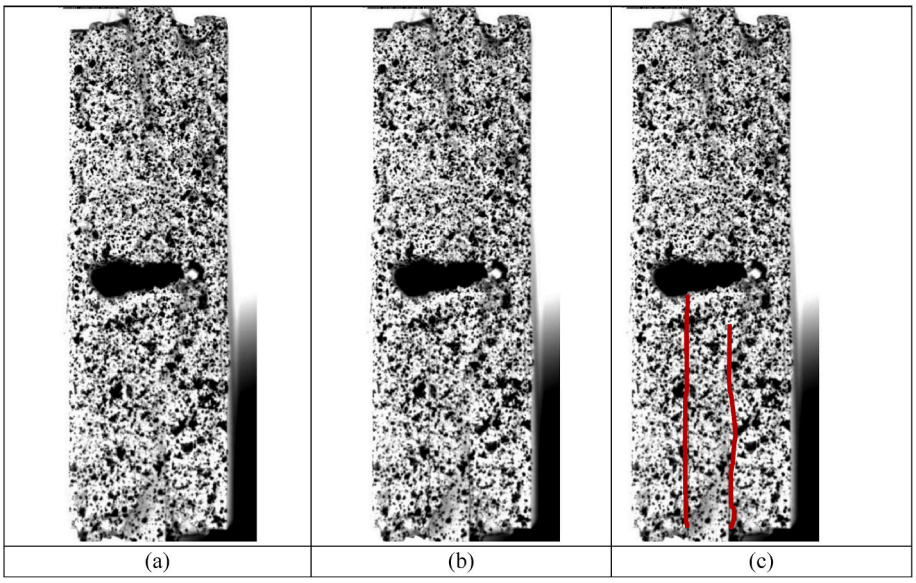

Fig. 17. Detailed view of the failed adhesive area, test CS4#1: a) absence of cracks before failure; b-c) presence of cracks at failure.

for the parameter l.

In fact, the time evolution of l can be associated with a pseudo-potential dissipation φ given by the sum of the rate-dependent and rate-independent terms (a positive homogeneous function), as shown in Eq. (5), where η is a positive viscosity parameter function of the adhesive layer thickness and I_B denotes the indicator function of a set B, i.e. $I_B = 0$ if $x \in B$ and $I_B = \infty$ otherwise.

$$\varphi(\dot{l}) = \frac{1}{2}\eta \dot{l}^2 + I_{]0,\infty[}(\dot{l}) \tag{5}$$

Furthermore, the term $I_{]0,\infty[}$ forces the crack length to assume non-negative values, so the crack length can only increase, making the degradation process of the adhesive irreversible. In order to impose unilateral contact (non-penetration condition) in the asymptotic expansion, the adhesive is considered as a soft material, following the Kachanov-type material, only in tension. The layer between the interphase and the adherents is considered perfect to ensure continuity in the interface separation and the stress vector. The interphase volume of the adhesive is replaced by an interface S of normal unit n using a suitable asymptotic expansion. After some manipulations, the following equations for the surface S can be obtained:

$$\sigma n = K(l)[u]_+ + \tau n \text{ on } S \tag{6}$$

$$\tau[u].n = 0, \tau \leq 0, [u].n \geq 0 \text{ on } S \tag{7}$$

$$\overline{\eta}\dot{l} = \left(\overline{\omega} - \frac{1}{2}K_{,l}(l)[u]_+.[u]_+\right)_+ \text{ on } S \tag{8}$$

In Eqs. (6)–(8), the symbol $[u]$ denotes the jump in the displacement field across the interface S and σ the Cauchy stress tensor. Furthermore, the symbol $()_{,l}$ denotes the partial derivate in l, $()_+$ which is the positive part of a function, i.e. $[u]_+ = [u]$ if $[u].n \geq 0$, $[u]_+ = [u] - [u].n$ if $[u].n \leq 0$. The parameter $\overline{\eta}$ is the limit of $\eta\varepsilon$ for $\varepsilon \to 0$ as well as $\overline{\omega}$ the limit of $\omega\varepsilon$.

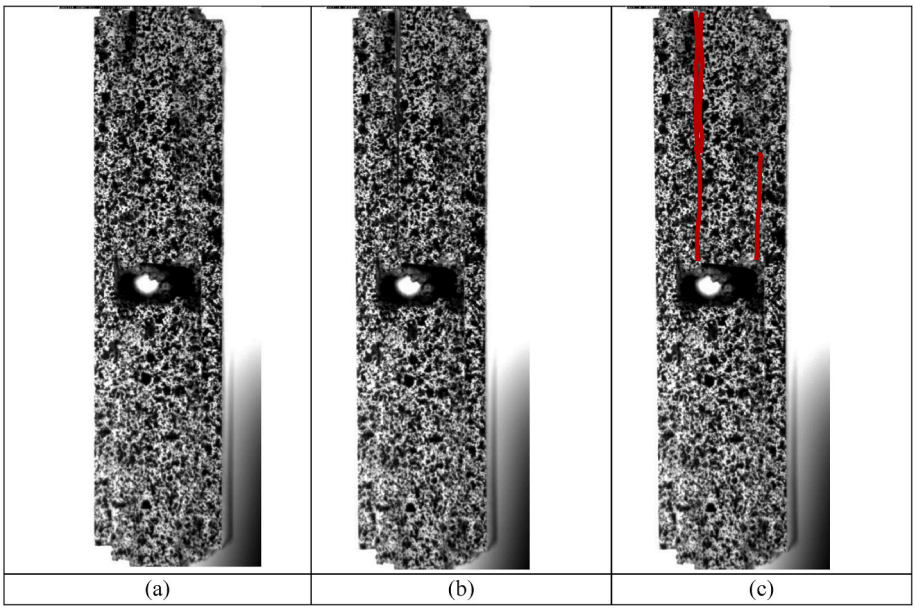

Fig. 18. Detailed view of the failed adhesive area, test CS2#2: a) absence of cracks before failure; b-c) presence of cracks at failure.

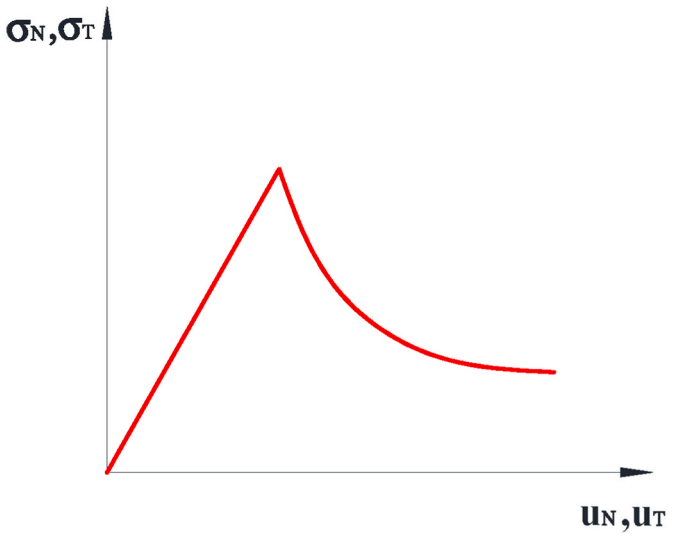

Fig. 19. Interface constitutive law for normal and tangential stress components.

Further information on the procedure used can be found in Ref. [39] as well as for the damage theories in Refs. [3,4,44].

As can be understood, Eqs. (6)–(8) describe an interface constitutive law as shown in Fig. 19. The law undoubtedly describes a spring-like interface model with non-linear damage evolution. As mentioned above, Eq. (8) represents the evolution of the parameter l by a simple derivation of a quadratic pseudo-dissipation potential, where the coefficient ω is a negative parameter such as Dupré energy. Furthermore, the damage process only starts when the elastic work is greater than a given value ω which is a function of the thickness of the adhesive. The interface stiffness tensor K can store the initial characteristics of the interphase such as geometry and mechanical properties. The homogenisation technique and the asymptotic approach lead to the following expression of the tangential and normal stiffness (Mode I and II) for an adhesive interface:

$$K_N(l) = \frac{3E_N S}{16l^3(1-v^2)} \tag{9a}$$

$$K_T(l) = \frac{3E_T S(2-v)}{32l^3(1-v^2)} \tag{9b}$$

where E_T is Young's modulus of the adhesive and v its Poisson ratio.

The power of this model is that it describes the behaviour of the adhesive through an interface model where the stiffness of the adhesive can change as a function of the variable damage.

To facilitate the understanding of the imperfect interface model, a conceptual diagram is provided in Fig. 20.

4.1. Validation of the theoretical model

The imperfect interface described in section 3 has been implemented in the commercial finite element software COMSOL Multiphysics [47]. To verify its accuracy and robustness, several simulations were performed and compared with the experimental results of double lap shear bonded joints subjected to different loading conditions.

The steel plates were modelled as an isotropic linear elastic material whose properties are given in Table 2. The adhesive layers, on the other hand, are replaced by a thin interface equation whose mechanical properties are given in Tables 3 and 4

Due to the presence of a plane of symmetry *y-z*, only a central part of the specimen was modelled with appropriate boundary conditions, thus optimising the analysis time. The specimen was fixed at the end of the steel plate, reproducing the experimental test conditions, and the load was applied on the opposite side.

After a mesh sensitivity study on the global behaviour of the specimen under tensile loading, a number of 12,273 3D tetrahedral elements were selected as shown in Fig. 21. In addition, the mesh details are given in Table 9 within the convergence test results (the chosen control parameter was the force, *F*, evaluated at the failure displacement for the case M4#1).

The description of the Mode II damage parameters and, in particular, the evaluation of the crack length taking into account the presence of diffuse cracks is summarised in Table 9. In particular, the damage length l_0 has been evaluated using Eq. (9b). More specifically, by solving Eq. (9a) as a function of l, it is possible to obtain Eq. (10). In this case, the slope of the experimental curve K_T is considered to determine the initial crack length l_0.

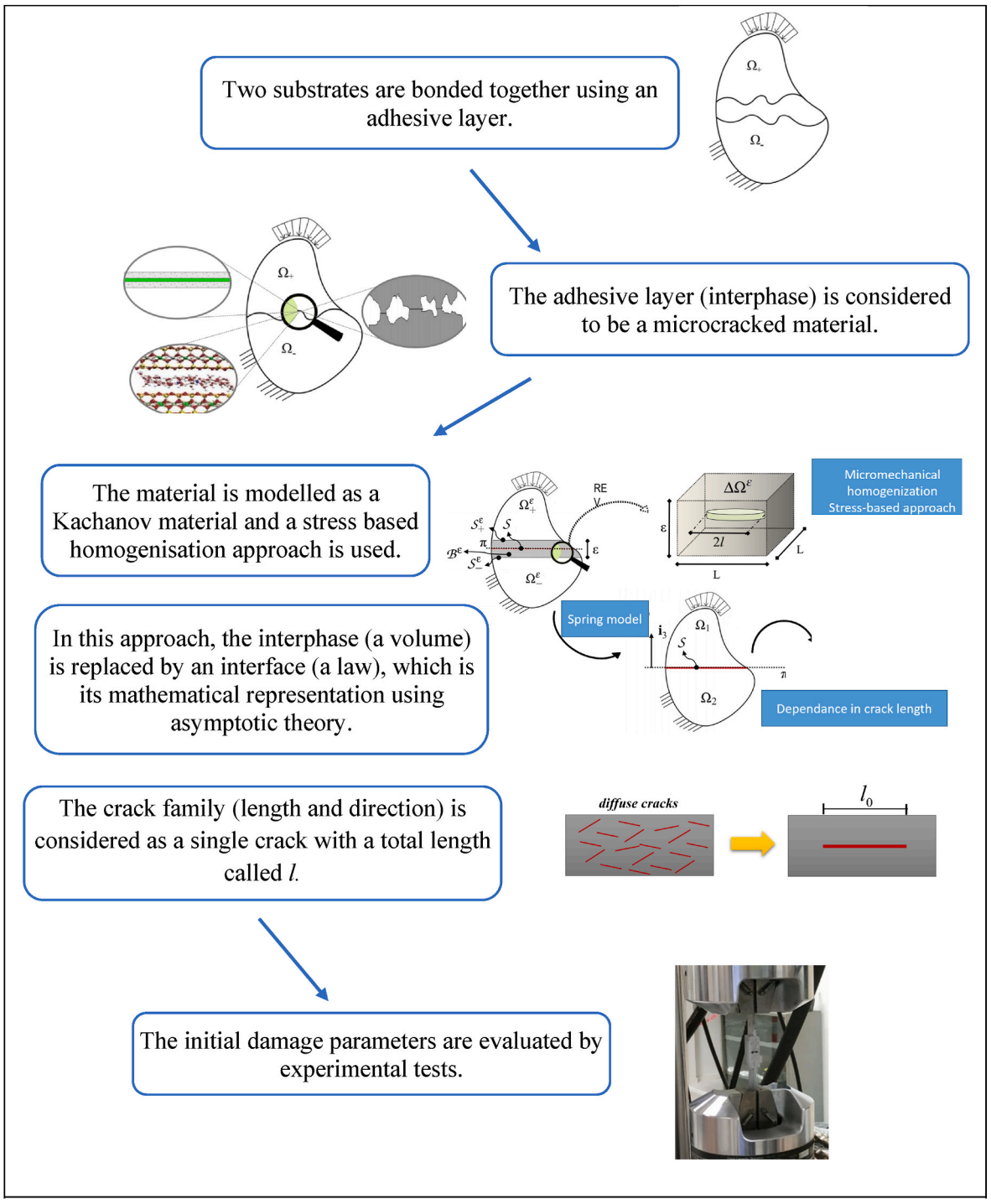

Fig. 20. Conceptual diagrams of the imperfect interface model [46].

$$l_0 = \left(\frac{3E_T S(2-v)}{32K_T(1-v^2)}\right)^{\frac{1}{3}} \tag{10}$$

It is important to note that the diffuse cracks present in the original adhesive layer can be considered as a single large crack of length l. The value of l_0 reported in Table 10 underlines how the presence of initial cracks is a function of the volume of adhesive material. The model parameters $\overline{\eta}$ and $\overline{\omega}$ have been calibrated from experimental data from static tensile tests on adhesive bonded assemblies and are reported in Table 10. It is important to underline that the identification process of the two model parameters has been obtained by comparing the global behaviour of the simulated tests with the experimental ones. In fact, the parameter $\overline{\eta}$ influences the shape of the interface law while the parameter $\overline{\omega}$ is representative of the area under the curve σ_T -u_T. It is worth noting that the model parameters control the post-peak behaviour after the elastic limit and the energy threshold above which damage is initiated, respectively.

Once the damage parameters have been defined, the spring equations (see Eqs. (6) and (7)) can be applied in the FEM model between two metal elements representing the adhesive layers.

Numerical results were obtained by applying the load in force control according to the load paths described in section 2.2. The comparison

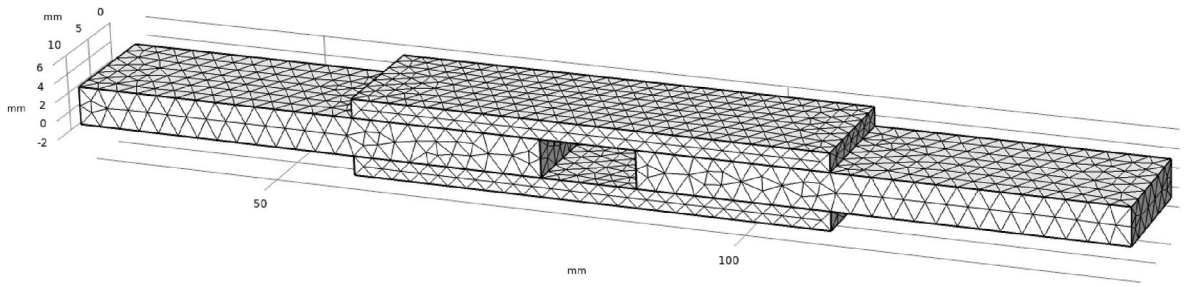

Fig. 21. Mesh detail of double lap shear adhesive joint.

Table 9
Mesh detail.

Number of elements	Experimental result Fu [KN]	FEM result Fu [KN]
535	9.976	9.987
2098		9.980
2793		9.978
4933		9.977
12273		9.976

Table 10
Damage parameters in the function of adhesive thickness.

Thickness t_a (mm)	Initial damage length l_0 (mm)	$\overline{\eta}$	$\overline{\omega}$
2	14.87	$5.0e^4$	$5.6e^4$
4	15.18	$1.8e^2$	$6e^4$

between experimental and numerical data is shown in the following figures: Fig. 22 shows the calculated and the corresponding experimentally measured force-displacement relationship curves for the CF4#3 double lap adhesive bond with an adhesive thickness of 4 mm under cyclic first-path loading; Fig. 23 shows the calculated and the corresponding experimentally measured force-displacement relationship curves for the CS4#2 double lap adhesive bond with an adhesive thickness of 4 mm under cyclic second-path loading; Fig. 24 shows the calculated and corresponding experimentally measured force-displacement relationship curves for the double lap adhesive joint CF2#2 with an adhesive thickness of 2 mm under cyclic first-path load, and Fig. 25 shows the calculated and corresponding experimentally measured force-displacement relationship curves for the double lap adhesive joint CS2#3 with an adhesive thickness of 2 mm under cyclic second-path load.

Comparison of the force-displacement curves computed by the current model with the corresponding experimental values for specimens CF4#3 and CF2#2 show good agreement, as well as for specimens CS4#2 and CS2#3. Indeed, an acceptable difference in terms of displacement can be found at failure for the comparisons shown in Figs. 23 and 25, which refer to experimental tests CS4#2 and CS2#3, respectively.

It is clear from the above comparisons that the imperfect model can accurately predict the above adhesive responses at all loading levels up to failure, demonstrating the robustness and accuracy of the method for all loading conditions applied to the specimens.

4.2. Numerical analysis

Using the imperfect interface model presented in Section 4, a numerical analysis has been developed to predict the failure load associated with double lap shear joints at varying adhesive moduli of elasticity. The geometric dimensions of the double lap shear joints are given in Fig. 2, while the mechanical properties of the steel plates are

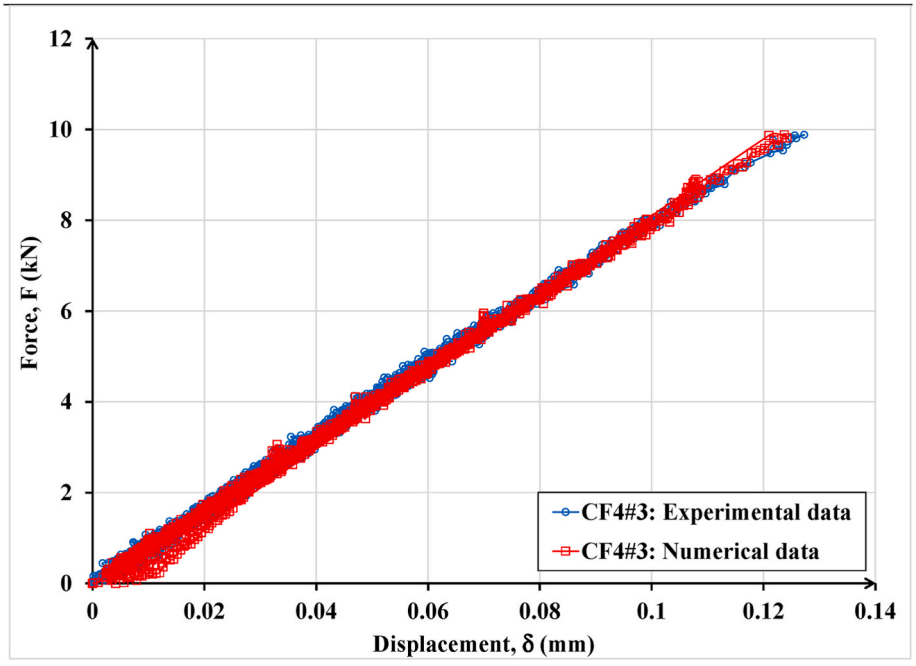

Fig. 22. Comparison of the calculated and experimental force-displacement curve for specimen CF4#3.

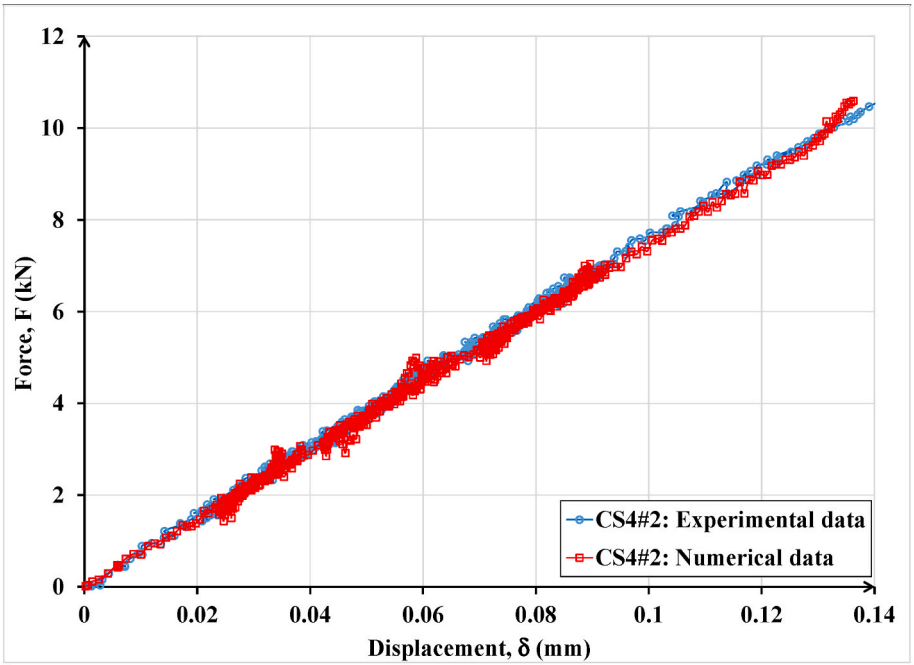

Fig. 23. Comparison of the calculated and experimental force-displacement curve for specimen CS4#2.

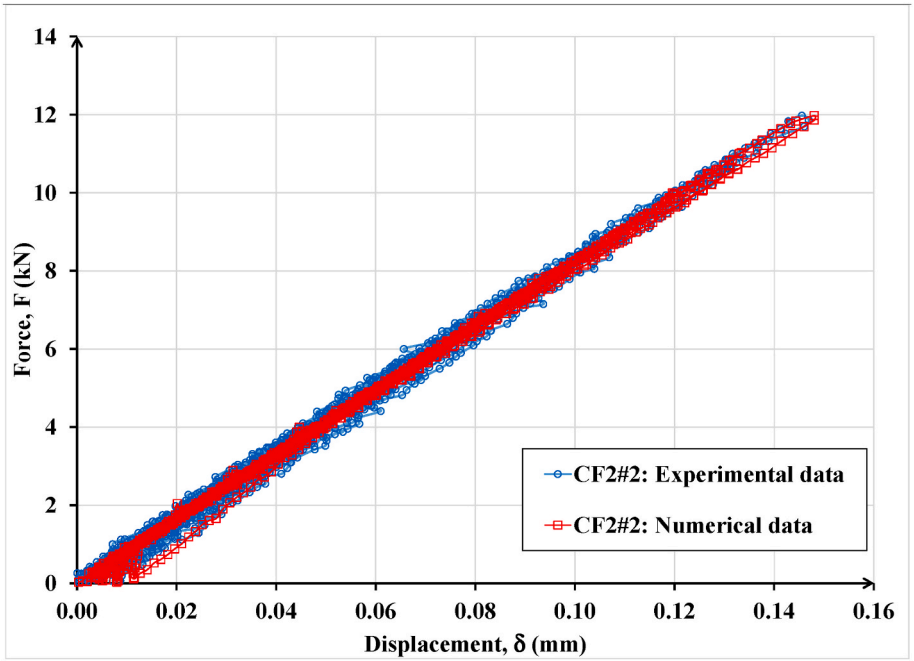

Fig. 24. Comparison of the calculated and experimental force-displacement curve for specimen CF2#2.

given in Table 2. The predictive analysis was carried out for two adhesive thicknesses: 2 and 4 mm. The numerical simulations were carried out under displacement control using the finite element model validated in the previous section 4.1 where all the details of the simulation method are reported.

Several types of adhesives were used in the numerical investigations, and their mechanical properties are given in Table 12. The numerical results obtained, expressed in terms of failure load versus adhesive Young's modulus, are summarised in Fig. 26.

The results presented in Fig. 26 are intended to provide a qualitative assessment of the failure load using adhesives characterised by different values of Young's modulus that may be available on the market.

As can be seen from Fig. 26, the response in terms of failure load of double lap shear joints is highly non-linear when the mechanical properties of the adhesive are varied.

5. Adhesive mechanical properties in mode I and II loading

In a previous work presented by some of the authors [4], the mechanical properties in terms of stiffness and crack length were evaluated for bonded joints subjected to Mode I loading, and are recalled here to provide, together with the current investigation, a complete characterization of the adhesive properties in Mode I and II, useful for FEM modelling and analysis.

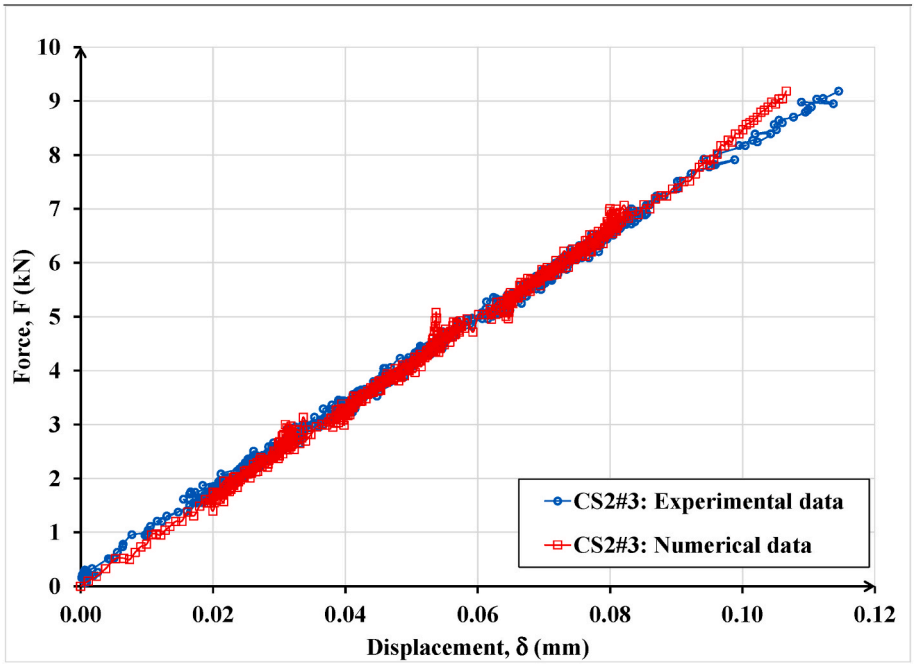

Fig. 25. Comparison of the calculated and experimental force-displacement curve for specimen CS2#3.

Table 12
Mechanical properties of adhesives.

Adhesive	Young's Modulus [MPa]	Tensile Strength [MPa]	Shear Strength [MPa]
Kemiepox 148 [48]	3300	62	16
Sicomin Isobond [49]	4500	62	14
Adesilex Pg1 [50]	6000	30	18
Sikadur30 [36]	11200	26–31	16–19

In this section, the adhesive stiffness in Mode II has been calculated from the mean value of the shear stress versus displacement curve, allowing comparison with the experimental results in Mode I.

The Mode I and II adhesive properties are summarised in Table 13, where the stiffness K and initial damage length l_0 have been evaluated for several thicknesses t_a. It is important to emphasise that the stiffness in Mode I and Mode II has been obtained from the elastic experimental curves in terms of stress-displacement, which can be represented by Eqs. (11) and (12) below:

$$K_I = \frac{F}{S_\perp \delta} = \frac{\sigma}{\delta} \tag{11}$$

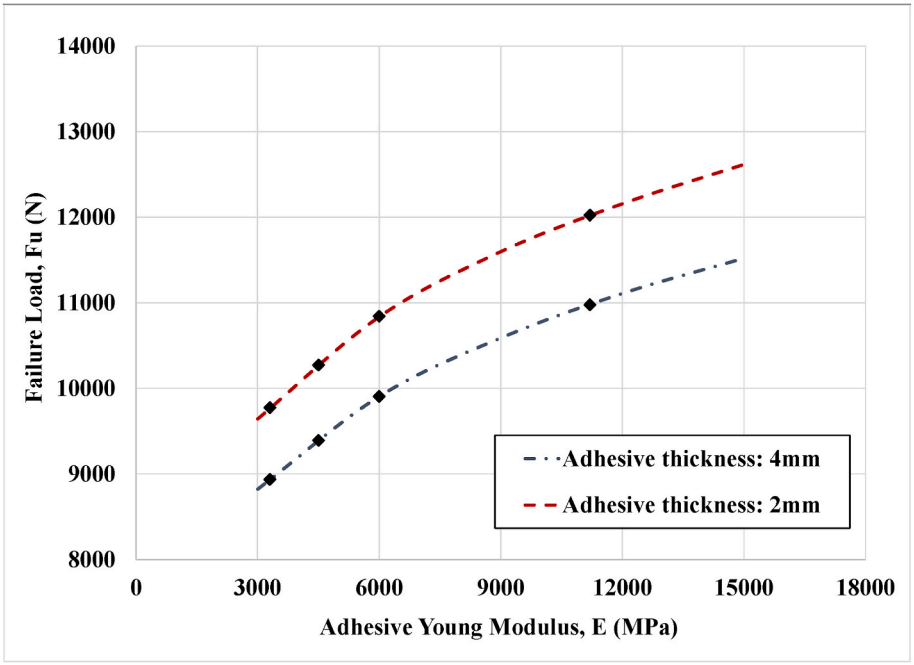

Fig. 26. Failure load when Young's modulus of the adhesive is varied.

Table 13
Comparison of the adhesive experimental properties in Mode I and II.

Mode	t_a	K	Initial damage length
	[mm]	[N/mm^3]	l_0 (mm)
I	1	341	11.44
	5	298	12.33
	10	243	12.96
II	2	67	14.87
	4	75	15.18

$$K_{II} = \frac{F}{S_{\parallel}\delta} = \frac{\tau}{\delta} \tag{12}$$

where $S_{\perp}$ and $S_{\parallel}$ represent the perpendicular and parallel adhesive surface to the applied force F.

6. Conclusion

At the Laboratory of Mechanics and Acoustics (LMA) in Marseille, an experimental program has been carried out on double lap shear bonded joints. Various load paths were applied to the adhesive specimens to evaluate their performance in the presence of severe loading conditions. In particular, the adhesive joints were subjected to different cycles characterised by low and high force levels, which could occur during the lifetime of any structure. Finally, an imperfect interface model was introduced to provide a design method capable of studying and predicting the behaviour of adhesive bonds under different load regimes.

The experimental results and numerical data supported the following conclusions.

- Two adhesive thicknesses were chosen, 2 and 4 mm, which can be easily reproduced in the field. The experimental results show how adhesive thickness affects the strength and stiffness of double lap shear joints. In particular, the best performance is obtained for the lower adhesive thickness.
- The influence of load-unload cycles up to 30% of the ultimate load was negligible in terms of bond stiffness and strength but became most important as the percentage of ultimate load increased.
- The percentage of residual displacement increases significantly as the load/unload cycles approach the ultimate load, providing a clear quantification of the damage suffered by the adhesive material.
- The damage parameter l_0, which represents the presence of internal cracks increases with the thickness of the adhesive layers.
- A parametric analysis was carried out to define the non-linear response of the bonded joint in terms of failure load at varying adhesive properties.
- Mechanical properties of bonded joints under Mode I and Mode II loading conditions have been provided.
- The proposed imperfect interface model undoubtedly represents a predictive method for studying the behaviour of bonded joints subjected to load cycling. The very good agreement between the experimental and numerical results underlines the power and robustness of the method, which introduces it as a design tool in the analysis of adhesive joints subjected to severe external loading.

Declaration of competing interest

The authors declare that they have no known competing financial interests or personal relationships that could have appeared to influence the work reported in this paper.

Data availability

Data will be made available on request.

Acknowledgement

This project has received funding from the European Union Horizon 2020 research and innovation programme under the Marie Sklodowska-Curie grant agreement No 843218-ASSO (Adhesive connection for Secondary Structures in Offshore wind installations). The authors would also like to thank the company BW Ideol for its financial support. The authors wish to commemorate Prof. Franco Maceri, for his commitment to teaching and research, which has promoted the Italian-French collaboration that is still continuing.

References

[1] Kwon JS, Choi DG, Park JS, Lee YS. Adhesive bonded composite laminate double lap joint and progressive failure analysis. In: Eccm – 18th European conference on composite materials; June 2018.
[2] Saleh MN, Saeedifar M, Zarouchas D, De Freitas ST. Stress analysis of double-lap bi-material joints bonded with thick adhesive. Int J Adhesion Adhes 2020;97:102480. https://doi.org/10.1016/j.ijadhadh.2019.102480.
[3] Maurel-Pantel A, Lamberti M, Raffa ML, Suarez C, Ascione F, Lebon F. Modelling of a GFRP adhesive connection by an imperfect soft interface model with initial damage. Compos Struct 2020;239:112034. https://doi.org/10.1016/j.compstruct.2020.112034.
[4] Lamberti M, Maurel-Pantel A, Lebon F, Ascione F. Cyclic behaviour modelling of GFRP adhesive connections by an imperfect soft interface model with damage evolution. Compos Struct 2022;279:114741. https://doi.org/10.1016/j.compstruct.2021.114741.
[5] Yang Y, Niscaia H, Chastre C, Silva AGM. Bond characteristics of CFRP-to-steel joints. J Constr Steel Res 2017;138:401–19. https://doi.org/10.1016/j.jcsr.2017.08.001.
[6] Volkersen O. Die Nietktraftverteilung in Zugbeanspruchen mit Konstanten Laschenquerschrittem. Luftfahrtforschung 1938;15(1–2):41–7.
[7] Goland M, Reissner E. The stresses in cemented joints. J Appl Mech 1944;11:17–27. https://doi.org/10.1115/1.4009336.
[8] Hart-Smith LJ. Adhesive-bonded scarf and stepped-lap joints. NASA Langley Report CR 1973;112237.
[9] Banea MD, da Silva LFM. Adhesively bonded joints in composite materials: an overview. Proc Inst Mech Eng Part L J Mater Des Appl 2009;23:1–18. https://doi.org/10.1243/14644207JMDA21.
[10] Budhe S, Banea MD, de Barros S, da Silva LFM. An updated review of adhesively bonded joints in composite materials. Int J Adhesion Adhes 2017;72:30–42. https://doi.org/10.1016/j.ijadhadh.2016.10.010.
[11] da Silva LFM, Rodrigues TNSS, Figueiredo MAV, de Moura MFSF, Chousal JAG. Effect of adhesive type and thickness on the lap shear strength. J Adhes 2006;82:1091–115. https://doi.org/10.1080/00218460600948511.
[12] Seong MS, Kim TH, Nguyen KH, Kweon JH, Choi JH. A parametric study on the failure of bonded single-lap joints of carbon composite and aluminium. Compos Struct 2008;86:135–45. https://doi.org/10.1016/j.compstruct.2008.03.026.
[13] Reis PNB, Ferreira JAM, Antunes F. Effect of adherend's rigidity on the shear strength of single lap adhesive joints. Int J Adhesion Adhes 2011;31:193–201. https://doi.org/10.1016/j.ijadhadh.2010.12.003.
[14] Vallée T, Tannert T, Murcia-Delso J, Quinn DJ. Influence of stress-reduction methods on the strength of adhesively bonded joints composed of orthotropic brittle adherends. Int J Adhesion Adhes 2010;30:583–94. https://doi.org/10.1016/j.ijadhadh.2010.05.007.
[15] Li J, Yan Y, Zhang T, Liang Z. Experimental study of adhesively bonded CFRP joints subjected to tensile loads. Int J Adhesion Adhes 2015;57:95–104. https://doi.org/10.1016/j.ijadhadh.2014.11.001.
[16] Kim JH, Park BJ, Han YW. Evaluation of fatigue characteristics for adhesively-bonded composite stepped lap joint. Compos Struct 2004;66:69–75. https://doi.org/10.1016/j.compstruct.2004.04.023.
[17] Jen YM, Ko CW. Evaluation of fatigue life of adhesively bonded aluminium single-lap joints using interfacial parameters. Int J Fatig 2010;32:330–40.
[18] Jen YM. Fatigue life evaluation of adhesively bonded scarf joints. Int J Fatig 2012;36:30–9. https://doi.org/10.1016/j.ijfatigue.2011.08.018.
[19] Tang JH, Sridhar I, Srikanth N. Static and fatigue failure analysis of adhesively bonded thick composite single lap joints. Compos Sci Technol 2013;86:18–25. https://doi.org/10.1016/j.compscitech.2013.06.018.
[20] Kang MH, Choi JH, Kweon JH. Fatigue life evaluation and crack detection of the adhesive joint with carbon nanotubes. Compos Struct 2014;108:417–22. https://doi.org/10.1016/j.compstruct.2013.09.046.
[21] Ayatollahi MR, Samari M, Razavi SMJ, da Silva LFM. Fatigue performance of adhesively bonded single lap joints with non-flat sinusoid interfaces. Fatig Fract Eng Mater Struct 2017;40:1355–63. https://doi.org/10.1111/ffe.12575.
[22] Razavi SMJ, Ayatollahi MR, Samari M, da Silva LFM. Effect of interface non-flatness on the fatigue behavior of adhesively bonded single lap joints. In: Proceedings of the institution of mechanical engineers, Part L: journal of materials: design and applications, vol. 233; 2019. p. 1277–86.
[23] Pereira AM, Reis PNB, Ferreira JAM. Effect of the mean stress on the fatigue behaviour of single lap joints. J Adhes 2017;93:504–13. https://doi.org/10.1080/00218464.2015.1110699.

[24] Boutara Y, Naimi S, Mezlini S, Carbas RJC, da Silva LFM, Ben Sik Ali M. Fatigue resistance of an aluminium one-component polyurethane adhesive joint for the automotive industry: effect of surface roughness and adhesive thickness. Int J Adhesion Adhes 2018;83:143–52. https://doi.org/10.1016/j.ijadhadh.2018.02.012.
[25] Saraç İ, Adin H, Temiz Ş. Experimental determination of the static and fatigue strength of the adhesive joints bonded by epoxy adhesive including different particles. Composites Part B 2018;155:92–103. https://doi.org/10.1016/j.compositesb.2018.08.006.
[26] Shahani AR, Pourhosseini SM. The effect of adherent thickness on fatigue life of adhesively bonded joints. Fatig Fract Eng Mater Struct 2019;42:561–71. https://doi.org/10.1111/ffe.12931.
[27] Pascoe JA, Zavatta N, Troiani E, Alderliesten RC. The effect of bond-line thickness on fatigue crack growth rate in adhesively bonded joints. Eng Fract Mech 2020;229:106959. https://doi.org/10.1016/j.engfracmech.2020.106959.
[28] Zhang J, Li HY, Li H, Jia H. Investigation on fatigue performance of adhesively bonded butt joints and multiaxial life estimation using stress-based failure models. Theor Appl Fract Mech 2020;107:102498. https://doi.org/10.1016/j.tafmec.2020.102498.
[29] Jahani K, Nobari AS. Identification of dynamic (Young's and Shear) moduli of a structural adhesive using modal based direct model updating method. Exp Mech 2008;48(5):599–611. https://doi.org/10.1007/s11340-008-9131-7.
[30] Meshki MM, Nobari AS, Nikbin K. Study of surface bonding imperfection effects on equivalent identified dynamic Young's and shear moduli using a modal based joint identification method. Mech Syst Signal Process 2015;52–53:1–16. https://doi.org/10.1016/j.ymssp.2014.08.012.
[31] Pazand K, Nobari AS. Identification of the effect of debonding on the linear and nonlinear effective damping of an adhesive joint. J Sound Vib 2016;380:267–78. https://doi.org/10.1016/j.jsv.2016.06.005.
[32] Tsukrov I, Kachanov M. Effective moduli of an anisotropic material with elliptical holes of arbitrary orientational distribution. Int J Solid Struct 2000;69:5919–41. https://doi.org/10.1016/S0020-7683(99)00244-9.
[33] Sevostianov I, Kachanov M. On some controversial issues in effective field approaches to the problem of the overall elastic properties. Mech Mater 2014;69:93–105. https://doi.org/10.1016/j.mechmat.2013.09.010.
[34] Kackanov M, Sevostanov I. Micromechanics of materials, with application, vol. 249. Springer; 2018. https://doi.org/10.1007/978-3-319-76204-3.
[35] Bruno G, Kachanov M, Sevostianov I, Shyam A. Micromechanical modelling of non-linear stress-strain behaviour of polycrystalline microcraked materials under tension. Acta Mater 2019;164:50–9. https://doi.org/10.1016/j.actamat.2018.10.024.
[36] SikaDur30 technical data sheet. URL:http://fra.sika.com/dms/getdocument, ; 2020.
[37] ASTM D3528 – 96. Standard test method for strength properties of double lap shear adhesive joints by tension loading. September 2002;10:1996.
[38] Nigro E, Di Ludovico M, Bilotta A. Experimental investigation of FRP-concrete debonding under cyclic actions. J Mater Civ Eng 2011;23(4):360–71. https://doi.org/10.1061/(ASCE)MT.1943-55330000173.
[39] Lebon F, Rizzoni R. Asymptotic behavior of a hard thin linear elastic interphase: an energy approach. Int J Solid Struct 2011;49:441–9. https://doi.org/10.1016/j.ijsolstr.2010.10.006.
[40] Benveniste Y, Miloh T. Imperfect soft and stiff interfaces in two-dimensional elasticity. Mech Mater 2001;33(6):309–23. https://doi.org/10.1016/S0167-6636(01)00055-2.
[41] Hashin Z. Thermoelastic properties of fiber composites with imperfect interface. Mech Mater 1990;8(4):333–48. https://doi.org/10.1016/0167-6636(90)90051-G.
[42] Raffa ML, Lebon F, Rizzoni R. Derivation of a model of imperfect interface with finite strains and damage by asymptotic techniques: an application to masonry structures. Meccanica 2018;53:1645–60. https://doi.org/10.1007/s11012-017-0765-3.
[43] Rekik A, Lebon F. Homogenization methods for interface modeling in damaged masonry. Adv Eng Software 2012;46:35–42. https://doi.org/10.1016/j.advengsoft.2010.09.009.
[44] Bonetti E, Bonfanti G, Lebon F, Rizzoni R. A model of imperfect interface with damage. Meccanica 2017;52:1911–22. https://doi.org/10.1007/s11012-016-0520-1.
[45] Orefice A, Mancusi G, Dumont S, Lebon F. Experimental/numerical study on the interfacial damage of bonded joints for fibre-reinforced polymer profiles at service conditions. Technologies 2016;4. https://doi.org/10.3390/technologies4030020. in line.
[46] Raffa ML, Lebon F, Vairo G. Normal and tangential stiffnesses of rough surfaces in contact via an imperfect interface model. Int J Solid Struct 2016;87:245–53. https://doi.org/10.1016/j.ijsolstr.2016.01.025.
[47] COMSOL Multiphysics® v. 5.6. Stockholm, Sweden: COMSOL AB; 2020.
[48] Kemiepox 148 Cristal technical data sheet. 2020. URL: https://www.poolkemie.it/fileadmin.
[49] Sicomin Isobond SR 5030/SD 503x technical data sheet. URL:https://sicomin.com/datasheets/product-pdf1254.pdf, ; 2018.
[50] Adesilex PG1 technical data sheet. URL: https://www.mapei.com/it/it/prodotti-e-soluzioni/prodotti/dettaglio/adesilex-pg1-rapido; 2020.